ACADEMIA ROMÂNĂ
Revue Roumaine de Chimie
https://www.icf.ro/rrch/

Rev. Roum. Chim.,
2023, *68*(3–4), 165–171
DOI: 10.33224/rrch.2023.68.3-4.06

Dedicated to Dr. Maria Zaharescu
on the occasion of her 85th anniversary

OPTICAL AND ELECTRICAL PROPERTIES OF AL-DOPED ZNO THIN FILMS DEPOSITED BY SOL-GEL METHOD

Madalina NICOLESCU[a*], Mihai ANASTASESCU[a*], Jose Maria CALDERON MORENO[a], Hermine STROESCU[a], Maria COVEI[b], Irina ATKINSON[a], Susana MIHAIU[a] and Mariuca GARTNER[a]

[a]"Ilie Murgulescu"Institute of Physical Chemistry, Romanian Academy, 202 Splaiul Independentei, 060021, Bucharest, Romania.
[b]"Transilvania" University of Brasov, 29 Eroilor Bd, 500036 Brasov, Roumania

Received November 22, 2022

The multilayer (10 layers) Al doped ZnO (AZO) thin films were deposited on glass substrate by sol-gel & dipping method. X-Ray diffraction measurements showed that the AZO films were polycrystalline with a hexagonal wurtzite structure. The morphological properties of the films were analyzed by atomic force microscopy showing continuous and homogeneous film, completely covering the substrates. The thickness, optical constants, optical band gap (E_g) and transmittance (T) of AZO films were assessed by spectroscopic ellipsometry on UV-vis-NIR spectral range. The AZO film has high transmittance above 80% in the visible region and the optical band-gap energy around 3.7 eV. The electrical characteristics regarding conductivity, mobility and carrier concentrations, were measured by Hall Effect measurements (van der Pauw method). The bulk carrier concentration of the AZO film with 10 layers was found to be 1.16×10^{19} cm^{-3}. The vibrational bands were obtained by Raman analysis. Defects due to oxygen vacancies in the prepared AZO films were evidenced by photoluminescence spectroscopy (PL). The optical and electrical properties of the AZO thin films proved the possibility to be used in optoelectronic applications.

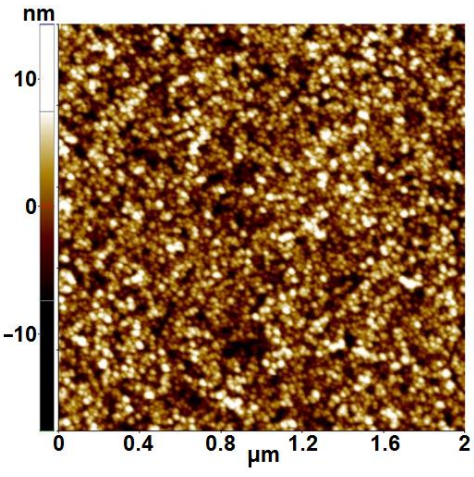

INTRODUCTION

ZnO is a very attractive semiconductor material which exhibits a hexagonal wurtzite structure, with wide band gap (3.37 eV) at room temperature, large exciton binding energy (60 meV) and strong luminescence emission ultraviolet (UV) domain. The other advantages of ZnO is nontoxic material, high chemical stability, low material cost, low resistivity, high transparency in the visible region but also facility. Due to these properties ZnO is a promising material used for fabrication of microelectronic and optoelectronic devices comparable with indium tin oxide.[1-7] ZnO thin films are processed using methods such as chemical vapor deposition,[8] spray pyrolysis,[9]

* Corresponding author: mnicolescu@icf.ro; manastasescu@icf.ro , Tel: +40213167912

thermal evaporation,[10] r.f. magnetron sputtering,[11, 12] and sol-gel method.[13-15] The sol-gel is a low cost deposition method which offers the possibility to obtain oxide films with thickness of nanometric scale, with controlled stoichiometry, good reproducibility, uniformity and doping. Based on these advantages, multilayer AZO thin films were deposited on glass substrates by dipping technique. The properties (structural, optical and electrical) of AZO film have been investigated by X-ray diffraction (XRD), atomic force microscopy (AFM), Spectroscopic Ellipsometry (SE), Hall Effect measurements, Raman and Photoluminescence (PL) spectroscopy.

RESULTS AND DISCUSSION

1. Structure and morphology

1.1. XRD

In Fig. 1 shows the XRD pattern of the AZO film deposited on glass substrate. The diffraction lines in the XRD pattern originated from (100), (002), (101), (102), (110), (103), and (112) reflections of hexagonal ZnO crystal structure according to the PDF Card no 00-036-1451 confirm the polycrystalline nature of the film.. Crystallites sizes of the (002) peak were obtained from the Scherer's formula is indicated in Table 1.

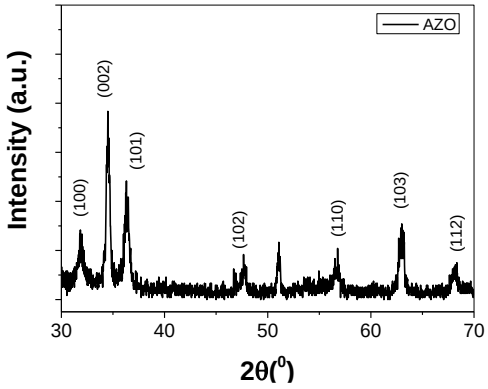

Fig. 1 – XRD-ray diffraction pattern of the AZO film deposited on glass.

The AZO film deposited on the glass substrate is oriented along the *c*-axis (002) (Fig.1). Furthermore, a shift toward the higher value of the diffraction line corresponding to the (002) plan is observed compared to the diffraction line reported in PDF Card no 00-036-1451.

The calculated lattice parameters with the standard deviation in the brackets are presented in Table 1. A slight decrease in the lattice parameters compared to those reported in the PDF card is observed, probably due to the replacement of Zn^{2+} ions by Al^{3+} ions during the formation of AZO film. The ionic radius of the Al^{3+} (r_{Al3+} = 0.54 Å) is smaller than that of the Zn^{2+} (r_{Zn2+} = 0.74 Å). The calculated crystallite size along the (002) direction was 24 nm.

Table 1

Lattice parameters and crystallite size of AZO film

Sample	Lattice parameters (Å)		Crystallite size (002) (nm)
	a = *b*	*c*	
AZO	0.3248 (0.3)	0.5182 (0.4)	24 (0.4)
ZnO 00-036-1451	0.3250	0.5207	–

1.2. AFM results

Figures 2(a and b) displays the topographic 2D and 3D images of the AZO films with 10 layers, deposited on glass, scanned over an area of (2μm × 2μm).

The AZO film deposited on glass (Fig. 2) exhibit a uniform and homogeneous structure of small grains, of 35 nm diameter, as revealed by the diameter histogram in Fig. 2c (fitted by a Gaussian function). The AZO film shows a smooth topography, characterized by a root mean square roughness of 3.77 nm. No defects as exfoliations or cracks were remarked in larger scales AFM images (10μm × 10 μm – not shown here) suggesting that the AZO films are continuous and have a good adherence to the substrate.

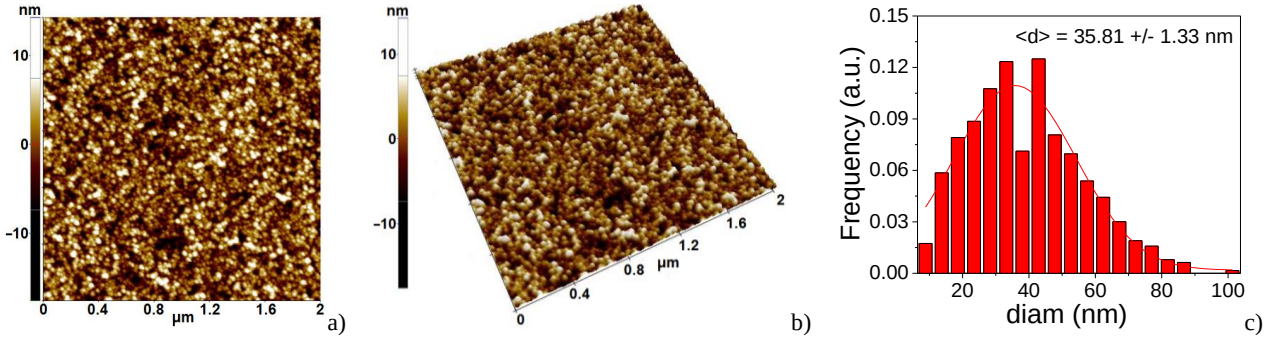

Fig. 2 – 2D (a) and 3D (b) topographic AFM images, registered at the scale of (2μm × 2μm) for the AZO films deposited on glass and diameter histogram of the surface particles (c).

2. Optical and electrical properties

A good agreement between the experimental and calculated ellipsometric parameters (ψ and Δ) measured in the 300–1700 nm range for AZO thin films deposited on glass is shown in the Fig. 3. The thickness (d_{film}), surface roughness (d_{rough}) and the optical constants (n, k) resulted from the best fit by modeled of the ellipsometric data with a 3 layer model: (air/surface roughness layer/AZO film/ substrate). The AZO film was modelled with General Oscillators model using Tauc-Lorentz oscillators and the roughness layer by effective medium approximation (EMA) model[16, 17] consisting in 50% film and50% voids. The band gap (E_g) value obtained by Tauc formula.[18]

The SE resulted are presented in the Table 2.

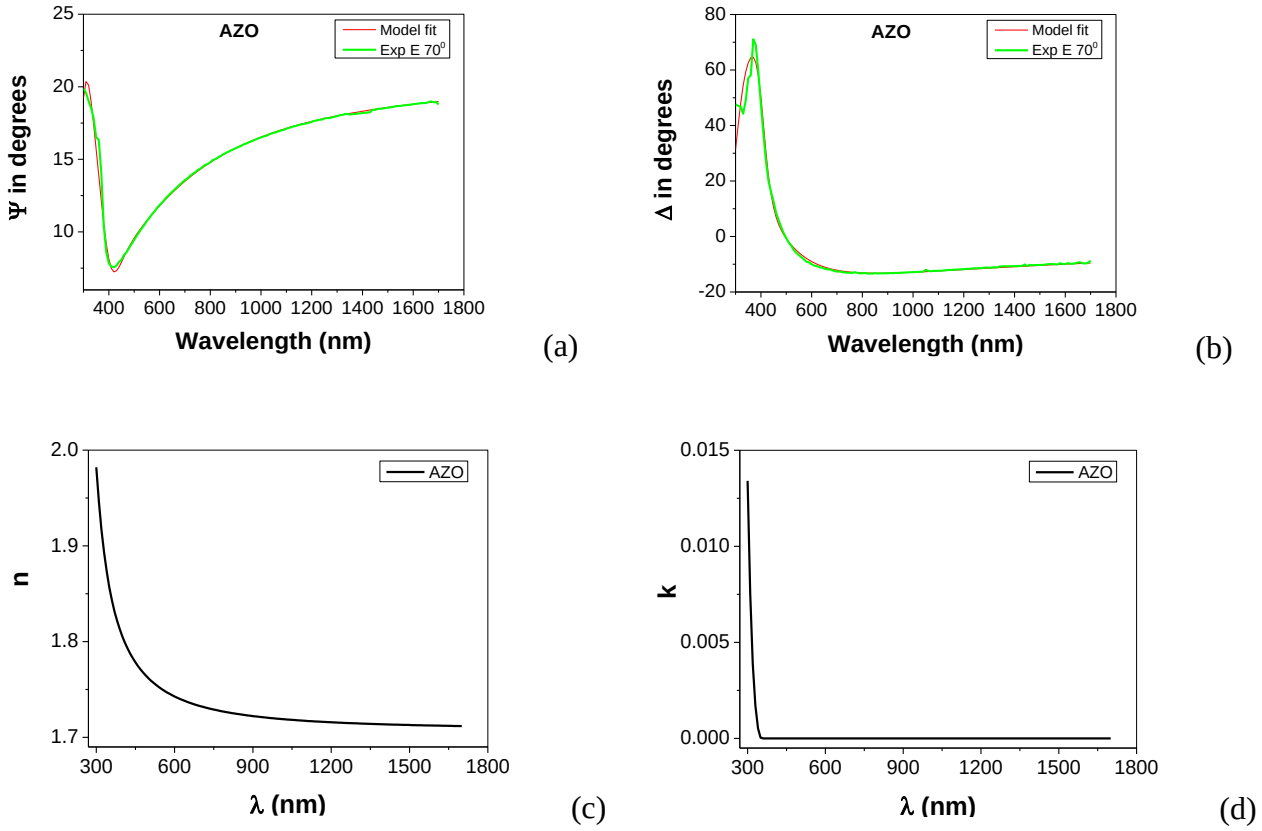

Fig. 3 – Experimental and calculated spectra of ellipsometric parameters ψ(a) and Δ(b) and the optical constants n (c) and k (d) for AZO film deposited on glass.

Optical transmission spectrum of the doped AZO film measured in the 250–1700 nm, it is shown in Fig. 4. It can be seen that the analyzed AZO film have a good transmittance (80%) in visible domain and over 88% in near-infrared domain.

The electrical parameters: carrier concentration (N_D), mobility (μ) and resistivity (ρ), determined from Hall Effect measurements, are presented in Table 3. The values of the carrier concentration of the order 10^{19} cm^{-3} was reported Jannane et al. and. Kumar *et al.*,[19, 20] and can be attributed to the quality of the crystallite which indicates a decrease in the defects in the film.

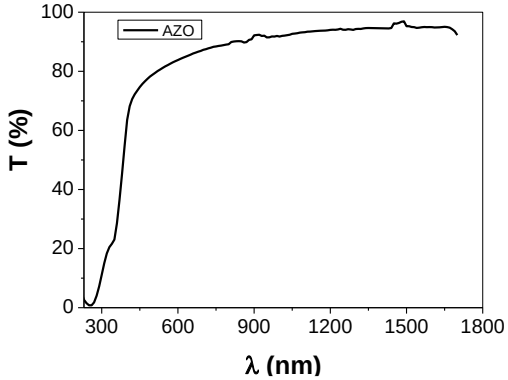

Fig. 4 – Transmission spectra of the AZO film deposited on glass.

Table 2

Parameters determined by SE analysis of AZO film on glass

d_{film} (nm)	d_{rough} (nm)	n*	T* (%)	E_g (eV)
75.1	2.6	1.74	84.93	3.63

*Note that n and T values were calculated at λ = 630 nm.

Table 3

Electrical parameters of the AZO film on glass

Sample	N_D (cm^{-3})	ρ (Ωcm)	μ (cm^2/Vs)	σ (1/Ωcm)
AZO	1.16×10^{19}	8.42×10^{-2}	6.37	11.87

In conclusion, the results obtained in the two analyzes demonstrated that the AZO multilayer film (10 layers) is suitable the properties required for optoelectronic applications such as low extinction coefficient in the visible range, large band gap, high transparency, respectively resistivity and good conductivity.

3. Raman analysis

Figure 5 shows the Raman spectra of AZO film deposited on glass. It is known that crystalline ZnO has eight sets of optical phonon modes at the Γ point in the Brillouin zone, Γ_{opt}, expressed as $\Gamma_{opt} = A_1$ (IR, R) $+E_1$ (IR, R) + $2E_2$ (R)+$2B_1$.[21] The active modes in infrared and Raman are A_1 and E_1 and it are split into transverse optical (TO) and longitudinal optical (LO) phonons modes.[21, 22] Also, the E_2 modes are nonpolar Raman active at low (E_2^{low}) and high (E_2^{high}) frequencies. The E_2^{low} mode involves mainly Zn sublattice motion while E_2^{high} is associated with the vibration of oxygen atoms.[21] The B_1 mode is silent in pure ZnO and present two modes low (B_1^{low}) and high (B_1^{high}) frequencies which are nonactive Raman modes but can be activated by introducing defects or by doping with other elements.[21, 25]

The optical vibrational bands of AZO films deposited on glass are presented in Table 4

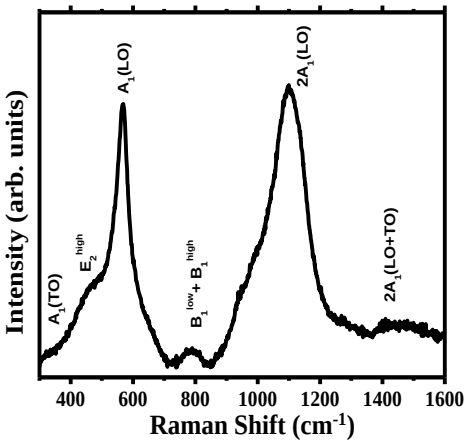

Fig. 5 – Raman spectra of AZO thin films deposited on glass

Table 4

Position of the Raman vibrational bands in the AZO thin films.

Symmetry	AZO (cm^{-1})	Literature (cm^{-1})[21-31]
A_1(TO)	335	331
E_2^{high}	445	447
A_1(LO)	570	573
$B_1^{low} + B_2^{high}$	790	809
$2A_1$(LO)	1101	1101
$2A_1$(LO+TO)	1457	1703

The Raman peak at 570 cm^{-1} corresponds with the A_1 (LO) mode of ZnO and is ascribed to the presence of defects such as oxygen vacancy and Zn interstitial defects.[22-24] The characteristic E_2^{high} mode of ZnO wurtzite structure is observed at 445 cm^{-1} as a shoulder of the A_1(LO) mode, as well as the weak A_1(TO) mode (335 cm^{-1}). The peak around at 800 cm^{-1}, reported also by Kumar[20] in sol-gel AZO films is attributed to the glass substrate, is assigned to the silent $B_1^{low} + B_2^{high}$ mode, activated by alumina doping[25]. The band at ~ 1100 cm^{-1} is assigned to the $2A_1$(LO) mode and the weak 1450 cm^{-1} band is attributed to $2A_1$(LO+TO) combination of the A_1 optical modes.[24-26,30,31]

4. Photoluminiscence analysis

ZnO is an important luminescent material for its emissions in UV, blue, green and red spectral range, which can lead to valuable industrial applications, mainly in the field of optoelectronic devices. The modification of the luminescence (intensity and position) can be obtained by doping ZnO with various metals.[13, 22-31]

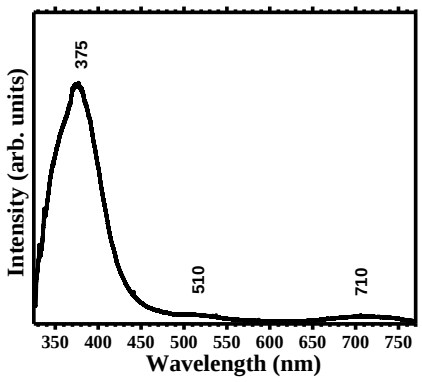

Fig. 6 – PL spectra of AZO thin films deposited on glass

The photoluminescence spectra of our AZO film excited by 325 nm at room temperature are presented in Fig. 6. Three emission peaks is observed a strong peak centered at 375 nm in UV range due to near-band-edge (NBE) emission of the ZnO and the green emission peak at 510 nm attributed the visible emission was attributed to the defects such as oxygen vacancies, zinc vacancies, interstitial oxygen and interstitial Zinc.[23-25] The band at 710 nm (near IR) corresponds defect related emissions.[26-28]

The values of PL emission peaks of the AZO thin film observed in our study is in good agreement with in the literature data.[21-31]

EXPERIMENTAL

Film preparation

Al doped Zinc oxide thin films (multilayer) have been deposited onto glass substrate by a sol-gel dipping method. The starting solution was prepared from Zinc acetate dihydrate-Zn $(CH3COO)_2 \times 2H_2O$ (ZAD), aluminum nitrate nonahydrate $Al(NO_3)_3 \times 9H_2O$ (ANN), absolute ethyl alcohol-CH_3CH_2OH and triethanolamine-N(CH_2-CH_2OH) (TEA). Zinc and aluminum solutions of 0.1 M and were obtained by dissolving of ZAD and ANN into absolute ethyl alcohol.

Zinc acetate solution was stirred at 60˚C for 15 minutes then TEA was slowly added drop wise in molar ratio of TEA/ZAD=1/5. The Al-Zn-sol was obtained by adding the appropriate quantity of ANN solution to the zinc acetate solution, so that finally represents 0.5% aluminum atoms in the Al-Zn mixture.

The thermal treatment of the deposited films was realized at 500˚C for 5 min, with a heating rate of 5 ºC/min. For multilayer coatings (up to 10 layers) after each deposition the same thermal treatment was applied. Finally, the multilayer samples deposited onto glass substrate were additionally annealed at 500˚C for 1 hour.

Characterization methods

The crystallinity of AZO films was studied by XRD analysis. XRD patterns were recorded using a Rigaku Ultima IV diffractometer, with Cu Kα radiation (λ = 1.5406 Å), operating at 40 kV and 30 mA equipped with thin film attachment for grazing incidence X-ray measurements, at an incidence angle ω = 0.5°. XRD diffractograms were recorded with the scan step of 0.02º and scan speed of 5 º/min over a range of 25-70°. Rigaku's PDXL software package,

connected to the ICDD database was used for the phase identification and lattice parameter calculation. Crystallite size was calculated using Scherrer's equation along (002) direction.

AFM measurements were performed to examine the surface morphology of the AZO films. All measurements were carried out in the non-contact mode, with an XE-100 apparatus from Park Systems, using sharp tips, NCHR model (Nanosensors^{TM}) with ~8 nm tip radius, ~125 μm length, ~30 μm mean width, thickness ~ 4 μm, ~ 42N/m force constant and ~330 kHz resonance frequency. The topographical 2D AFM images were taken over the area of 10×10 μm^2 and 2×2 μm^2. Regarding the tilt correction and the evaluation of the root mean square roughness, the images were analyzed with XEI (v.1.8.0) Image Processing Program developed by Park Systems.

The optical properties of the films were studied by SE measurements using an Woollam VASE ellipsometer. The film thickness (d_{film}), optical constants (refractive index, *n*, and extinction coefficient, *k*), the band gap energy (E_g) and the transmission (*T*) were determined by measurements in the 300–1700 nm (UV-vis-NIR) spectral range. Measurements have been performed at room temperature, using the 70° as incidence angles with 10 nm wavelength step. WASE program from Woollam was used for multi-parameter fitting program in which an iterative least-squares method is used for minimizing the difference (mean square error – MSE) between of the experimental and theoretical data, the ellipsometric data analysis with an accuracy of ± 0.005.

The optical transmission measurements were performed at 0° incidence angle on the same apparatus

Raman and PL spectra were recorded in a Horiba Jobin Yvon LabRam HR spectrometer using a 325 nm excitation laser and a NUV 40× objective.

Carrier concentration, resistivity and mobility were determined based on Hall Effect performed at room temperature using the van der Pauw method by HMS-5000 system from Ecopia having a magnetic field of 0.55 T.

CONCLUSION

The AZO thin films were deposited by sol-gel and dipping method on glass substrate, and characterized by XRD, AFM, SE, Raman and PL measurements.

XRD revealed the good crystallization of multilayer AZO film deposited on glass by dip coating. A decrease of the lattice parameters with the doping was observed, suggesting the incorporation of Al into ZnO matrix, confirmed by Raman (peak at about 572 cm^{-1}) and PL (presence of NBE emission). AFM measurements showed uniform and homogeneous structure. The large band gap E_g= 3.63 eV, high transparency (>80%), low extinction coefficient in the visible range and the low resistivity (8.42 x10^{-2} Ωcm) recommend the use of AZO films to the fabrication the optoelectronic devices.

Acknowledgements The paper was carried out within the research program "Science of Surfaces and Thin Layers" of the "Ilie Murgulescu" Institute of Physical Chemistry. Romanian Government that allowed for the acquisition of the research infrastructure under POS-CCE O 2.2.1 project INFRANANOCHEM – No. 19/01.03.2009 is gratefully acknowledged.

REFERENCES

1. X.T. Hao, F.R Zhu, K.S. Ong and L.W. Tan, *Semicond. Sci. Technol.*, **2006,** *21*, 48-54.
2. M.A. Mahadik, Y.M. Hunge, S.S. Shinde, K.Y. Rajpure and C. H. Bhosale, *J. Semicond.*, **2015**, *36*, 033002.
3. Q. Simon, D. Barreca, A. Gasparotto, C. Maccato, E. Tondello, C. Sada, E. Comini, A. Devi and R.A. Fischer, *Nanotechnology*, **2012**, *23*, 025502.
4. T. Makino, C.H. Chia, T.T. Nguen, Y. Segawa, M. Kawasaki, A. Ohtomo, K. Tamura and H. Koinuma, *Appl. Phys. Lett.*, **2000**, *771*, 632–1634.
5. X. Zhang and R. Zhu , *J. Phys.: Conf. Ser.*, **2020** , *1549*, 042006.
6. Z. Fan, D.Wang, P.-C. Chang, W.-Y. Tseng and J.G. Lu, *Appl. Phys. Lett.* , **2004**, *85*, 5923.
7. M. Gabas,N.T. Barrett, J.R. Ramos-Barrado, S. Gota, T.C. Rojas and M.C. Lopez-Escalante, *Sol. Energy Mater. Sol. Cells*, **2009**, *93*, 1356–1365.
8. D.B. Potter, I.P. Parkin.and C.J. Carmalt, *RSC Adv.*, **2018**, *8*, 33164-33173.
9. S. Kurtaran, *Opt. Mater.*, **2021**, *114*, 110908.
10. O. M.Abdulmunem, M. J. M. Ali and E.S.Hassan, *Opt. Mater.*, **2020**, *109*, 110374.
11. M. Mickan, U.Helmersson and D. Horwat, *Surf.Coat. Technol.*, **2018**, *347*, 245-251.
12. M. Nicolescu, M. Anastasescu, S. Preda, J.M. Calderon-Moreno, H. Stroescu, M. Gartner, V.S. Teodorescu, A.V. Maraloiu, V. Kampylafka, E. Aperathitis and M. Modreanu, *J. Optoelectron. Adv. Mater.*, **2010**, *12*, 1343 – 1349.
13. E. Musavi, M. Khanlary and Z. Khakpour, *J. Lumin.*, **2019**, *216*, 116696.
14. A. Sharmin, S.Tabassum, M.S. Bashar and Z. H.Mahmood, *J. Theoretical and Applied Physics*, **2019**, *13*, 123–132.
15. S. R. Bhattacharyya and, S. Majumder, *Funct. Mater. Lett.*, **2010**, *3*, 111–114.
16. H.G. Tompkins, "WVASE32 Software Training Manual", J.A. Woollam Co., Inc., Lincoln, NE, USA, 2006.
17. "WVASE32® Software Manual", J.A. Woollam Co., Inc., Lincoln, NE, USA.
18. J. Tauc, R. Grigorovici and A.Vancu, *Phys. Status Solidi B*, **1966**, *15*, 627–637.
19. T. Jannane, M. Manoua, A. Liba, N. Fazouan, A. El Hichou, A. Almaggoussi, A. Outzourhit and M. Chaik, *J. Mater. Environ. Sci.*, **2017**, *8*, 160-168.
20. K.D.A. Kumar, S. Valanarasu, A. Kathalingam, V. Ganesh, M. Shkir and S. Al Faify, *Appl.Phys. A* , **2017**, *123*, 801.
21. J.Panda, I. Sasmal and T.K. Nath, *AIP Adv.*, **2016**, *6*, 035118.
22. M. Nicolescu, M. Anastasescu, S. Preda, H. Stroescu, M. Stoica, V.S Teodorescu, E. Aperathitis, V. Kampylafka,

M. Modreanu, M. Zaharescuand M. Gartner, *Appl. Surf. Sci.*, **2012**, *261*, 815–823.
23 S. Simeonov, A. Szekeres, D. Spassov, M. Anastasescu, I. Stanculescu, M. Nicolescu, E. Aperathitis, M. Modreanu and M. Gartner, *Nanomaterials*, **2022,** *12*, 19.
24 M.A.M. Ahmed, W.E. Meyer and J.M. Nel, *Mater. Sci. Semicond. Process.*, **2019**, *103*, 104612.
25 F.J. Manjon, B.Mari, J. Serrana and A.H. Romero, *J. Appl. Phys.*, **2005**, *97*, 053516.
26 M. Silambarasan, S. Saravanan and T. Soga, *Int. J. Chem Tech Res.*,**2014-2015**,*7*, 1644-1650.
27 M. Koyano, P.Q. Bao, L.T. Binh, L.H. Ha, N.N. Long and S. Katayama, *Phys. Stat. Sol. A*, **2002**, *193*, 125–131.
28 W.Bousslama, H. Elhouichet, B. Gelloz, B. Sieber, A. Addad, M. Moreau, M. Férid and N. Koshida, Jpn. *J. Appl. Phys***.**, **2012**, *51*, 04DG13.
29 R. Raji and K.G. Gopchandran, *J. Sci. Adv. Mater. Dev*., **2017**, *2*, 51–58.
30 I. Musa, N. Qamhieh and S.T. Mahmoud, *Results Phys.*, **2017**, *7*, 3552–3556.
31 R. Zhang, P.-G. Yin, N. Wang and L. Guo, *Solid State Sci.*, **2009**, *11*, 865–869.